Chemical Engineering Journal 285 (2016) 581–587

Contents lists available at ScienceDirect

Chemical Engineering Journal

journal homepage: www.elsevier.com/locate/cej

Chitin hydrogel reinforced with TiO_2 nanoparticles as an arsenic sorbent

María Luz Peralta Ramos [a], Joaquín A. González [a], Sabrina G. Albornoz [a], Claudio J. Pérez [b], María E. Villanueva [a], Sergio A. Giorgieri [a], Guillermo J. Copello [a,*]

[a] Universidad de Buenos Aires (UBA), Facultad de Farmacia y Bioquímica, Cátedra de Química Analítica Instrumental, IQUIMEFA (UBA-CONICET), Junín 956, C1113AAD Buenos Aires, Argentina
[b] Instituto en Investigaciones en Ciencia y Tecnología de Materiales, Universidad de Mar del Plata, (CONICET), Juan B. Justo 4302, CP7600 Mar del Plata, Argentina

HIGHLIGHTS

- A chitin hybrid gel was obtained without the need of crosslinkers.
- TiO_2 reinforces chitin gels endowing mechanical stability.
- TiO_2 endows chitin gels with arsenic adsorption capacity.
- Chitin–TiO_2 gels showed arsenic sorption capacity in natural waters.
- The chosen components make this material a promising low-cost sorbent.

GRAPHICAL ABSTRACT

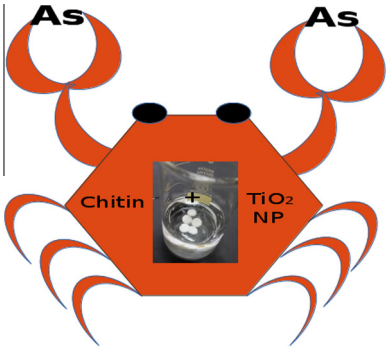

ARTICLE INFO

Article history:
Received 10 August 2015
Received in revised form 4 October 2015
Accepted 6 October 2015
Available online 19 October 2015

Keywords:
Chitin
Titanium dioxide nanoparticles
Arsenic
Removal
Hybrid material

ABSTRACT

In this work chitin hydrogels were reinforced with TiO_2 nanoparticles acting as fillers. The mechanical and physicochemical characteristics of these hydrogels were studied by oscillatory rheology, infrared spectroscopy (FTIR), Scanning Electron Microscopy (SEM) and Small Angle X-ray Spectroscopy (SAXS). Adsorption showed to be higher at pHs below the TiO_2 point of zero charge (pH ≈ 6.9). The equilibrium was achieved within 4 h following an Elovich kinetic model. The equilibrium assay showed a maximum capacity of 3.1 mg/g with better fitting for the Langmuir model. Moreover, the homogeneity/heterogeneity parameters of the Sips, Toth and Redlich–Peterson models were close to a value of 1, indicating a homogeneous sorbent/sorbate interaction. Typical natural water ions competed with As(V) for the sorption sites, being sulfate the most relevant interference. This interference was also evidenced in As(V) adsorption from natural water samples where the sorption capacity varied depending the anion composition of the sample. The reutilization of the hybrid gel was assessed up to five adsorption cycles.

1. Introduction

Arsenic presence in natural waters is a matter of concern in vast areas of Argentina, Chile, China, India, Bangladesh, among others countries. Arsenic water contamination is usually associated with non-urban zones where fast, easy application and low-cost answers are needed. With this aim several techniques have been studied, such as coagulation-coprecipitation, photocatalytic reduction, photocatalytic oxidation and adsorption using different materials [1–3].

Among As adsorbents, TiO_2 has been studied in different formats and sizes, from nanoparticles to micrometric range granular particles [4–6]. It is a non-toxic compound used in pharmaceutic,

* Corresponding author at: Química Analítica Instrumental, FFyB, UBA, Junín 956 – Piso 3 (C1113AAD), CABA, Argentina. Tel./fax: +54 11 49648254.
E-mail address: gcopello@ffyb.uba.ar (G.J. Copello).

http://dx.doi.org/10.1016/j.cej.2015.10.035
1385-8947/

cosmetic and biomedical products due to its biocompatibility [7]. However, the use of powdered TiO_2 in aqueous media requires laborious separation to prevent the leakage of the particles [1,8]. In this aspect, the development of hybrid materials represents a novel strategy for the mechanical reinforcement and chemical stability of the sorbent and the prevention of the particle leakage. Examples of these hybrids are polyurethane–keratin membranes, Chitin–Kraft lignin, chitosan–sulfydryl bearing graphene oxide, sil ica–alginate–xanthan gum, etc [9–12].

In the last years, chitin based hybrids have enhanced their applicability as biomaterials thanks to novel manipulation techniques which have overcome the polysaccharide low solubility [13,14]. Chitin is a cheap polysaccharide that can be extracted from shrimp, crab shell, fungi, as well as other invertebrates such as marine sponges [15,16]. Being a waste material from food industry it is a low-cost biopolymer which is also biocompatible, biodegradable and non-toxic [7]. Although less expensive and chemically more stable in comparison with its derivative chitosan, literature still shows few approaches dedicated to pure chitin derived hydrogel materials. Most of these studies use the potentially toxic crosslinker epichlorohydrin for the obtaining of reinforced materials, such as chitin/poly(vinyl alcohol) or chitin/clay nanotubes [17,18]. Other approaches achieve the material final structure either by lyophilization or by reinforcement with high loads of graphene oxide [19–21].

The aim of this work was to combine two low-cost, non-toxic and biocompatible compounds for the obtaining of a chemically and mechanically stable arsenic adsorbent. Herein, a chitin hydrogel reinforced with TiO_2 nanoparticles was developed for As(V) adsorption. Chitin and TiO_2 nanoparticles were chosen based in their lower cost in comparison with other polysaccharides and metal nanoparticles and the latter's high surface area and arsenic sorption capacity. The nanostructure of the composites was characterized using different spectroscopic techniques and the degree of reinforcement was assessed by a rheological analysis. The As (V) adsorption performance was evaluated by means of the influence of media pH, interaction time, sorption capacity, competing ions and reutilization. The sorption capacity was also assessed against natural water samples containing natural arsenic or spiked with known concentrations.

2. Experimental

2.1. Reagents and materials

Chitin from crab shells (DA: 92%; Mr ≈ 400,000) was obtained from Fluka (USA). Calcium chloride dihydrate was purchased from Anedra (Argentina); Methanol was acquired from Sintorgan (Argentina). $Na_2HAsO_4{\cdot}7H_2O$ was purchased from Mallincrodt. Arsenic concentration was verified against the appropriate dilution of the arsenic standard 1000 mg/L (Chem-Lab, Belgium). TiO_2 nanoparticles ($d \approx 30$ nm) (AEROXIDE TiO_2 P25, Evonik) were kindly donated by Evonik Degussa Argentina SA. Water was filtered and deionized with a Milli-Q, Millipore system (Milford, MA, USA). All other reagents were of analytical grade.

Tap-water was collected from Buenos Aires Autonomous City (Arg.) and well-water samples were collected from Chascomús city, Chivilcoy city, Pehuajo city, Trenque Lauquen city, Tortuguitas city (Buenos Aires province, Arg.). Tap-water samples were collected from household taps connected to the city water supply network. Well-water samples were collected from household taps connected to systems of water pumped from wells. Before collecting the samples water was let run for 5 min. Waters were stored at 4 °C until the assays and used without further treatment.

2.2. Preparation of chitin hydrogel and chitin–TiO_2 hybrid materials

The chitin suspension was obtained following the method proposed by Tamura et al. [13]. Briefly, in order to prepare a transparent calcium solvent, 42.5 g of calcium chloride dihydrate were suspended in 50 mL of methanol and refluxed for 30 min at 82 °C to a state of near-dissolution. One gram of chitin powder was suspended in the calcium solvent and refluxed for 2 h at 90 °C with stirring in a round-bottom flask attached to a Liebig condenser.

Different mass ratios of chitin and TiO_2 were mixed by thorough agitation in order to obtain three types of hybrid materials with different chitin to TiO_2 ratios (Chi:Ti): (10:1), (5:1) and (2.5:1).

The mixtures were poured between two glasses spaced by glass slides of known width and then submerged in methanol until they gelled. Finally, the gels were subjected to several water incubations in order to wash out all the methanol and $CaCl_2$ residues. Blank chitin gels without TiO_2 were obtained by a similar procedure and named Chi gels. The gels were cut in a certain geometry depending on the experiments.

2.3. Rheological behavior

Amplitude sweeps were performed first in order to determine the linear viscoelastic range (LVR). The elastic or storage modulus, G', the viscous or loss modulus, G'' and complex viscosity (η^*) of the studied materials were obtained in small-amplitude oscillatory shear flow experiments using a rotational rheometer from Anton Paar (MCR-301) provided with a CTD 600 thermo chamber. The tests were performed using parallel plates of 25 mm diameter and a frequency range of 0.1–500 s^{-1}. The measurements were carried out at room temperature (20 °C). All the tests were performed using small strains (γ = 3.0%) to ensure the linearity of the dynamic responses [22]. All the runs were repeated using different samples. The gap width used was 700–800 μm.

2.4. Scanning Electron Microscopy

Topography and size of samples were studied by Scanning Electron Microscopy (SEM). Images of freeze-dried and gold coated samples were taken using a Zeiss Supra 40. Secondary electron detector and Backscattered electron detectors were used for image acquisition. TiO_2 nanoparticle size was confirmed by deposition of powder and direct observation.

2.5. Spectroscopic characterization

FTIR transmission spectra were acquired in the range of 4000–400 cm^{-1} using a Fourier Transform Infrared Spectrometer (FTIR) (Nicolet 360). All samples were dried for 24 h at 60 °C prior to the KBr preparation in order to avoid water related bands interference. Chitin degree of acetylation (DA) was determined by the method proposed by Brugnerotto et al., which is based on the relationship between a reference band at 1420 cm^{-1} and the amide III band at 1320 cm^{-1} by applying the following equation: A1320/A1420 = 0.3822 + 0.03133DA [23].

The investigation of the ultrastructure of the nanocomposites was performed by Small Angle X-ray Scattering using the SAXS2 beamline of the National Synchrotron Light Laboratory (LNLS), Campinas, Brazil. The SAXS measurements were performed at room temperature in transmission geometry with λ = 1.55 Å (8 keV). The 2D SAXS spectra were detected on a marCCD 165 detector. A sample to-detector distance of 0.5 and 2 m and an exposure time of 60 s were used. The samples were placed with their surfaces perpendicular to the direction of the incident X-ray

beam and parallel to the X-ray detector. The scattering intensity (I) was measured as a function of the scattering vector (q) from 0.07 to 5.3 nm^{-1}. The background and parasitic scattering were determined by using an empty sample holder and were subtracted for each measurement. SASfit software was used for data analysis and curve fitting [24].

2.6. Adsorption experiments

Adsorption experiments were carried out by a batch method at room temperature (25 °C) with constant stirring (120 rpm). Discs of 6 mm diameter and 2 mm width (0.2 g) were added to aqueous solutions (5 ml) of As(V), ranging from 0.1 to 10 mg/L respectively. The effect of media pH, interfering ions, interaction times and adsorption isotherms were determined by sorbate decay in the solution supernatant. Arsenic determinations were performed using a Buck Scientific VGP 210 Atomic Absorption Spectrophotometer (E. Norwalk, CT, USA) by the electrothermal atomization method using pyrolytic graphite tubes. Nickel Nitrate (0.2%) was used as matrix modifier.

The interference of Cl^-, SO_4^{2-} and NO_3^- was studied between 10 and 100 mg/L in a solution containing 0.1 mg/L As(V). Adsorption of As(V) from natural water samples was tested with and without spiking of a known amount of As(V) depending on the initial concentration. Natural water ion composition studies were carried out on a Capillary Electrophoresis System with diode array detector (Agilent Technologies). Analysis parameters were used as described elsewhere [25].

The reutilization of the hybrid gels was assessed by subsequent incubations in 1 mg/L As(V) solutions. Between each adsorption cycle, the desorption was carried out by four washing steps in 0.1 M NaOH for 15 min and then four equilibration steps in ultrapure water for 15 min.

All adsorption assays were carried out in plastic vessels. Blank experiments were conducted in order to verify the absence of sorbate precipitation and/or adsorption to the walls of the vessels. All experiments and their corresponding measurements were conducted at least in triplicate under identical conditions and statistically analyzed by one-way ANOVA and Tukey Multiple comparison post test if ANOVA $p < 0.05$. R language and environment was used for statistical computing and graphics [26].

3. Results and discussion

3.1. Rheological behavior

The rheological behavior of the Chi gels and the Chi:Ti hybrids was studied in order to verify the reinforcement effect that is macroscopically observed in the hybrids (Fig. 1). In all materials, a gel-like behavior was confirmed by higher G' values than G'' ones, which implies a dominance of the elastic component over the viscous component. It can also be observed that the G' value of the material increases with the raise of TiO_2 content. The complex viscosity of all the gels decreases almost linearly with the increment of the frequency showing shear thinning behavior probably due to the structure of the hybrid polymer network (Fig. 1).

3.2. Microscopic structure

Chi gels and Chi:Ti hybrids were observed by SEM (Supplementary Data 1). On the SEM images acquired with a secondary electron detector it could be observed that Chi gels present a smooth surface with pores. With the addition of TiO_2 nanoparticles, the material is endowed with higher rugosity. In the Chi:Ti (2.5:1) image (Supplementary Data 1 d), it could also be observed aggregates of the nanoparticles, probably due to the high concentration of TiO_2. Whereas topography information can be obtained from secondary electrons, the detection of backscattered electrons (BSE) brings information from atomic number contrast. The BSE images of Chi gels and Chi:Ti hybrids are shown in Supplementary Data 2. The BSE images show that the nanoparticles aggregates tend to decrease in size and become more dispersed with the decrease of TiO_2 content in the hybrids.

3.3. Spectroscopic characterization

The IR spectra of the TiO_2 nanoparticles, Chi gels and Chi:Ti (5:1) in the range of 2000–800 cm^{-1} are shown in Supplementary Data 3. In the Chi gels spectra the bands corresponding to chitin structure could be observed. These bands are the amide I band at 1653 cm^{-1}, corresponding to the unresolved doublet accounting for C=O and C—N stretchings, the amide II band at 1558 cm^{-1} (N—H bending), at 1420 cm^{-1} (CH_2 bending), 1378 cm^{-1} (CH bending), 1313 cm^{-1} (amide III and CH_2 wagging) and the polysaccharide related bands at 1157 cm^{-1} (asymmetric bridge oxygen stretching), 1068 cm^{-1} and 1030 cm^{-1} (both from C—O stretching) [23,27]. The TiO_2 nanoparticles spectrum shows a band at 1638 cm^{-1} which accounts for the bending mode of hydroxyl groups associated to strongly adsorbed water to the titania surface [28]. No new bands could be observed on the Chi:Ti (5:1) spectrum, which indicates that no new chemical groups are formed during the hybrid synthesis. Nevertheless, the amide I band from chitin spectrum and the hydroxyl band from the nanoparticles are overlapped and both peaks appear joined in a broader peak with center at 1649 cm^{-1}.

The SAXS technique was used to obtain structural information of the gels network in the nanometric scale. Fig. 2 shows the SAXS profiles of Chi gel and Chi:Ti (5:1) hybrid gel. Chi gel scattering profile follows a power-law behavior in the q range of ~0.009–0.05 $Å^{-1}$, above which a short knee-like middle regime with a lower slope appears. This profile is found in disordered materials with at least two structural levels. In the low q region the Chi gel spectrum, fitted according to the relation $I(q) \sim q^{-\alpha}$, shows values of the exponent α near to 2.5. This behavior is indicative of scattering from fractal objects and would become from chitin chains free folding in the gel stage [29,30]. Within this range the Chi:Ti (5:1) hybrid spectrum shows a knee-like regime (0.009–0.3 $Å^{-1}$) which would account for larger structures than the ones observed in Chi gel profile. In Chi:Ti the (5:1) hybrid profile the power-law behavior is observed in the q range of ~0.03–0.2 $Å^{-1}$, presenting an α of 3.4. This value is related to surface fractals and denser network structures [30]. In this profile, the knee-like regime observed in Chi gel spectrum is less intense indicating a weaker contribution of this structure to the overall scattering.

With the aim of describing mass fractal morphologies, Beaucage proposed a unified equation that gives insight throughout multiple structural levels of disordered materials [31]:

$$I(q) \approx G\exp\left(\frac{-q^2R_g^2}{3}\right) + B\exp\left(\frac{-q^2R_{sub}^2}{3}\right)\left(\frac{1}{q^*}\right)^P + G_s\exp\left(\frac{-q^2R_s^2}{3}\right) + B_s\left(\frac{1}{q_s^*}\right)^{Ps}$$

where G and G_s are the Guinier prefactors for the larger and smaller structures respectively, R_g is the radius of gyration, B and B_s are prefactors specific to the power-law scattering, which are specified as the decay exponent P and P_s respectively, $q^* = q/[\mathrm{erf}(q\ k\ R_g/6^{1/2})]^3$ and $q_s^* = q/[\mathrm{erf}(q\ k_s\ R_s/6^{1/2})]^3$.

The adjustments of the Beaucage unified equation present a value of $R_g = 11.9 \pm 0.1$ nm and 28.1 ± 0.6 nm for the Chi gel and Chi:Ti profiles respectively. The R_g value obtained for the Chi gels

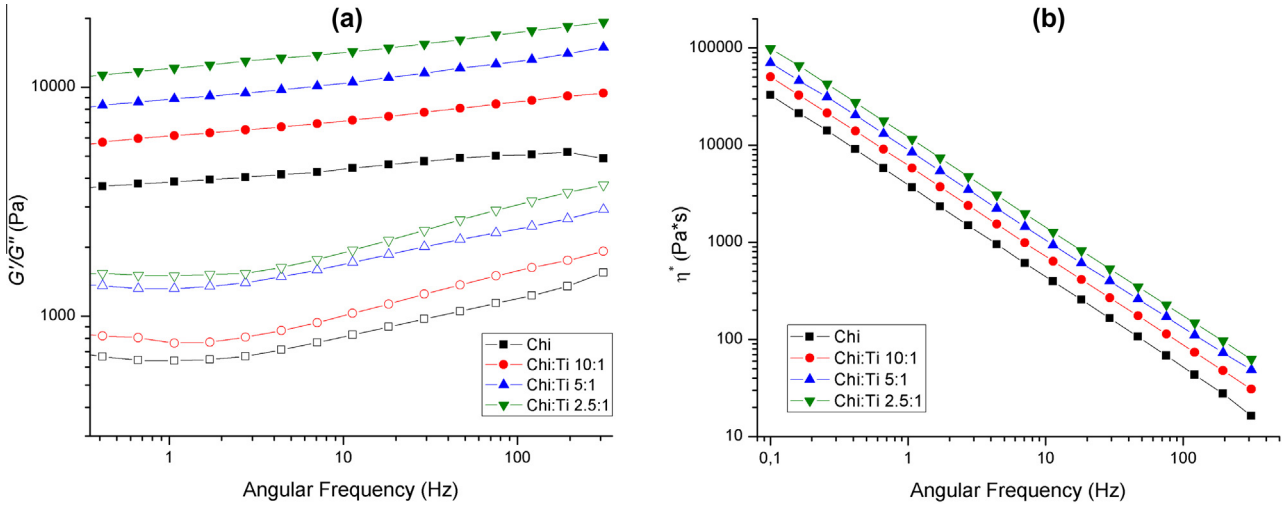

Fig. 1. Storage modulus (G') (solid symbols) and loss modulus (G'') (hollow symbols) frequency dependence (a) and complex viscosity of the Chi and Chi:Ti hybrids.

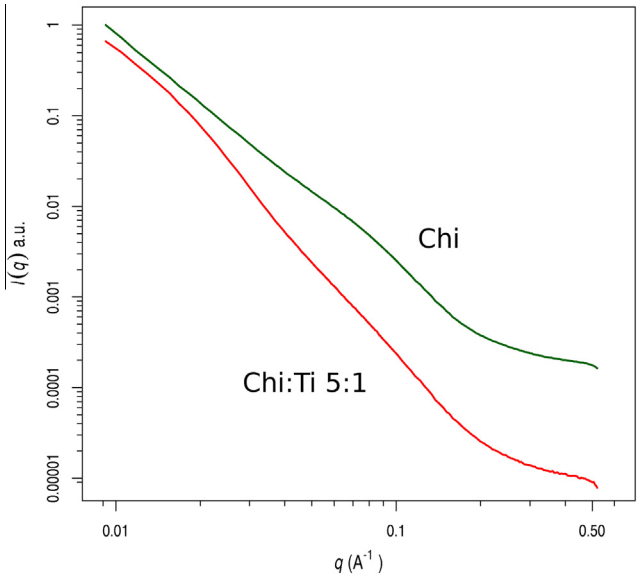

Fig. 2. SAXS profiles of Chi gels and Chi:Ti (5:1) hybrids.

would account for structures formed during the gel stage due to the interaction of the polymer chains, whereas the R_g value obtained for the Chi:Ti hybrid gel is related to the detection of TiO_2 nanoparticles with diameters around 30 nm. Moreover, the SEM image of the TiO_2 shows particle sizes around this value (Supplementary Data 4).

3.4. Effect of pH on adsorption behavior

The effect of media pH on the adsorption behavior was analyzed in the pH range 3–7 (Supplementary Data 5). Chi gels did not present adsorption capacity for As(V) at any pH. This highlights the fact that the addition of TiO_2 is not only relevant in the mechanical aspect but also in its As(V) sorption performance. Regarding the hybrids, media pH influenced As(V) adsorption mainly when sorption capacities at pH 3 and 5 are compared with the pH 7 ones (significantly different, $p < 0.05$). Comparing each hybrid behavior the adsorption at pH 7 was significantly different and lower than the corresponding one at pH 3 or 5. For the pristine TiO_2 the rise in adsorption capacity between pH 3 and 5 is more evident. At this pH range, As(V) presents several anionic forms, such as $AsO_2(OH)_2^-$, $AsO_3(OH)^{2-}$ and AsO_4^{3-}. Also, since the point of zero charge pH (PZC_{pH}) of TiO_2 is near 6.9, at this pH range TiO_2 presents a positively charged surface exposing Ti-OH_2^+ groups [4]. As a consequence, the main mechanism of As(V) adsorption would be the electrostatic attraction. This is also supported by the lack of change in the pH of adsorption solutions after incubation. A change in pH would be indicative of ionic exchange reactions rather than electrostatic attraction as proposed. Chi:Ti gels with (5:1) and (2.5:1) ratios did not present significant differences in their adsorption capacities neither at pH 3 or at 5 ($p > 0.05$, Tukey post-test). Although higher adsorption capacities were expected for the Chi:Ti (2.5:1) gels due to its higher TiO_2 content, probably the agglomerates seen in the SEM images are affecting the adsorption performance of this hybrid. Therefore, the Chi:Ti (5:1) hybrid, which contains less TiO_2 and is more homogeneous, and pH 3, which was the one with higher capacities, were chosen as the optimum conditions to perform the kinetic and equilibrium assays.

3.5. Adsorption kinetics

In order to characterize the kinetic behavior of the Chi:Ti (5:1) hybrid gel, the adsorption of As(V) over time was assessed. Kinetic modeling of this data was performed using the pseudo-first-order, pseudo-second-order, Elovich and the modified Freundlich equations in their non-linear forms [32–34]. Table 1 summarizes the kinetic parameters. The mathematical models are presented in Supplementary Data.

Goodness-of-fit of the non-linear models was evaluated by the corrected Akaike's information criteria (AICc) [35]. Smaller AICc values represent better curve fittings [35].

Fig. 3 shows the adsorption over time at pH 3. The material achieved equilibrium time within 4 h showing the best fitting for the Elovich model. This would indicate that the rate limiting step

Table 1
Kinetic parameters for As(V) adsorption.

Model	Parameter		Goodness-of-fit (AICc)
Elovich	α (μg/g h)	7 ± 3	−115.2
	β (g/μg L)	11 ± 1	
Modified Freundlich	k_F (L/g h)	0.368 ± 0.008	−114.9
	m	4.6 ± 0.5	
Pseudo-2nd order	q_{eq} (μg/g)	0.52 ± 0.02	−110.7
	k_2 (g/μg h)	7 ± 1	
Pseudo-1st order	q_{eq} (μg/g)	0.46 ± 0.01	−100.5
	k_1 (h^{-1})	2.4 ± 0.3	

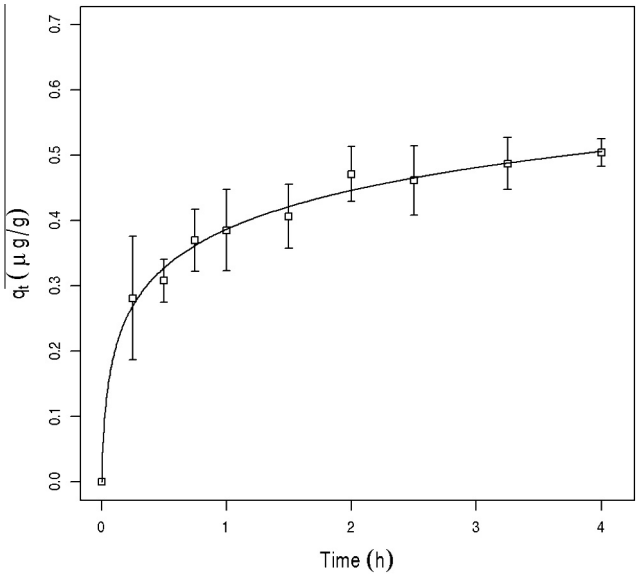

Fig. 3. As(V) adsorption over time at pH 3 using Chi:Ti (5:1) hybrids. Elovich model is presented. q_t (±SD, $n = 4$).

is the chemisorption process [32]. The second best fitting model was the Modified Freundlich's, which can describe kinetics controlled by intra-particle diffusion when m approaches a value of 2 [36]. In this case the obtained value was far from 2. Thus, the intra-particle diffusion process would play a negligible role in the adsorption kinetics of As(V) probably because adsorption takes place in the surface of the non-porous TiO_2 nanoparticle [4].

3.6. Adsorption isotherms

Adsorption isotherm data were obtained after equilibrium time was achieved, at pH 3 (Fig. 4). Adsorption capacities (q_{eq}) are expressed as the mass of sorbate per mass unit of sorbent (mg/g) and determined as follows: $q_{eq} = (C_0 - C_{eq})V/m$; where C_0 and C_{eq} are the initial and the equilibrium As(V) concentrations of the incubation solution respectively (mg/L), V is volume of solution (L) and m is the sorbent mass (g). Adsorption isotherm models were used to model equilibrium data. The two parameter models analyzed were the Langmuir, Freundlich and Dubinin–Radushkevich (D–R) models and the three parameter models were the Redlich–Peterson (R–P), Toth and Sips models [33,37–40]. Table 2 presents the results obtained from the fitted models. The mathematical models are presented in Supplementary Data.

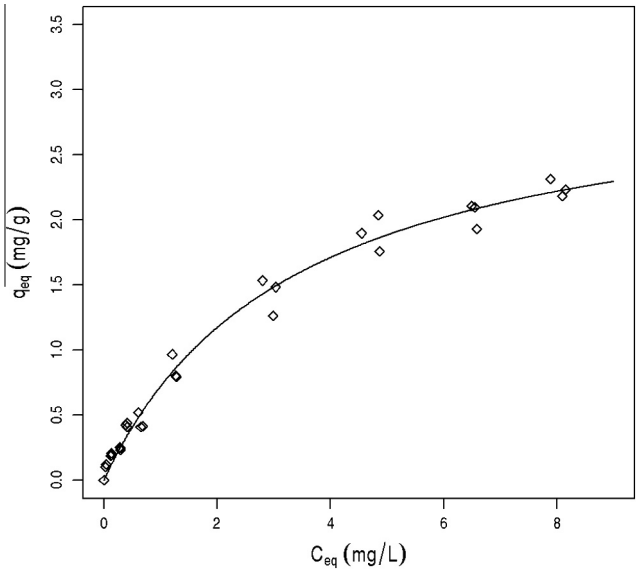

Fig. 4. Adsorption isotherm at pH 3 using Chi:Ti (5:1) hybrids. Langmuir model is presented. q_{eq} (±SD, $n = 3$).

The experimental data fitted better for the Langmuir isotherm model followed by the Sips model. The Langmuir model typically presents good adjustment for systems where the sorbate adsorbs on the sorbent in a monolayer to homogeneous adsorption sites [33]. This behavior could be expected for this system were chitin present negligible adsorption capacity for As(V). Therefore, anionic As(V) would be adsorbed homogeneously to the TiO_2 nanoparticle surface. Moreover, the homogeneity/heterogeneity parameters of the R–P, Sips and Toth models show a trend towards a value of 1, which would be indicative of a homogeneous adsorption process [40,41].

If the adsorbent surface is heterogeneous and homogeneous subregions are considered, an average free energy value could be calculated using D–R equation [42]. $E_{DR} = (2K_{DR})^{-1/2}$, where E_{DR} is the mean free energy of adsorption (kJ/mol). The mean free energy of adsorption can be indicative of the type of adsorption interaction. In an adsorption process where chemisorption prevails, such as in charge associated interactions, the magnitude of E_{DR} is in the range of 8–16 kJ/mol [42]. Lower values are related to physisorption processes and larger values have been reported for coordination or chemical reactions [42]. Taking into account that the Elovich kinetic model presents the best fitting and the E_{DR} was 11.9 kJ/mol, it could be assumed that As(V) adsorption onto the Chi:Ti hybrids is a homogeneous chemisorption process driven by electrostatic attraction between an anionic sorbate and the positive charge density of the sorbent surface.

3.7. Coexisting anions effect and natural water performance

Fig. 5 shows the influence of the concentration of coexisting anions in the adsorption capacity of As(V). Chloride, sulfate and nitrate were chosen since they are common anions of natural waters. The presence of these anions in a level of 10 mg/L reduces the adsorption capacity in 40% with respect to the one for ultrapure water ($q_{eq} = 0.1$ mg/g). Higher levels of Cl^- do not show higher reduction of As(V) adsorption capacity. This is not the case for the presence of NO_3^-, which decreases As(V) adsorption if it is

Table 2
Isotherm model parameters.

Model	Parameter		Goodness-of-fit (AICc)
Langmuir	q_m (mg/g)	3.1 ± 0.1	−53.6
	k_a (L/mg)	0.29 ± 0.03	
Sips	q_{mS} (mg/g)	3.7 ± 0.6	−52.7
	K_S (L/mg)	0.21 ± 0.08	
	n_S	0.89 ± 0.08	
Toth	q_{mT} (mg/g)	4 ± 1	−51.8
	b_T (L/mg)	0.29 ± 0.04	
	n_T	0.8 ± 0.2	
Redlich–Peterson	K_{RP} (L/mg)	1.0 ± 0.2	−51.6
	α_{RP} ((L/mg)^{nRP})	0.4 ± 0.2	
	n_{RP}	0.9 ± 0.1	
Dubinin–Radushkevich	q_{DR} (mg/g)	47 ± 6	−46.3
	K_{DR} (mol^2/kJ^2)	(3.5 ± 0.1) × 10^{-3}	
	E_{DR} (kJ/mol)	11.9 ± 0.2	
Freundlich	k (L/g h)	0.72 ± 0.02	−40.5
	n	0.57 ± 0.02	

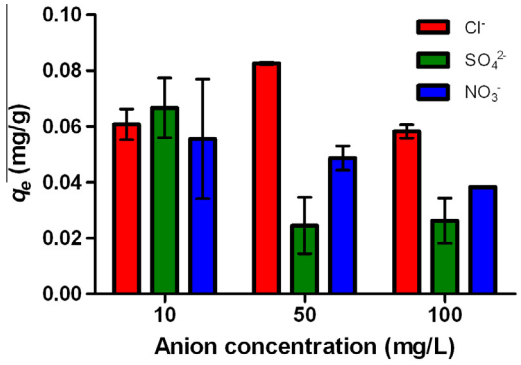

Fig. 5. Influence of the concentration of coexisting anions in As(V) adsorption capacity. q_{eq} (±SD, n = 3).

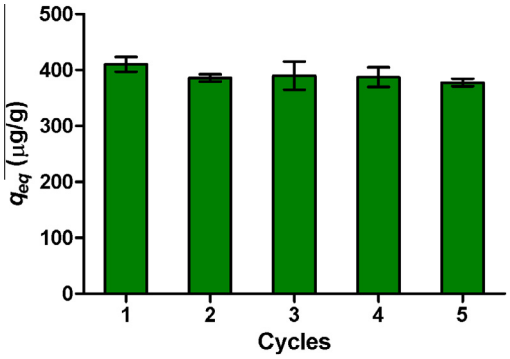

Fig. 6. Influence of reutilization cycles in the As(V) adsorption capacity of the Chi:Ti (5:1) hybrids. q_{eq} (±SD, n = 4).

present at higher levels. The steepest drop in As(V) adsorption is produced by the presence of sulfate anions, being around 75% when SO_4^{2-} is ⩾50 mg/L or higher. According to EPA water standards, the maximum Cl^-, SO_4^{2-} or NO_3^- content in drinking water should be 250 mg/L, 250 mg/L and 10 mg/L, respectively. Since low interference was detected for chloride, and nitrate interference is higher at concentrations which this anion should not exceed in drinking water, the content of sulfate anions should be considered as the most relevant interference for As(V) adsorption.

Table 3 shows the adsorption performance of natural or spiked As(V) from tap or well-water. The highest adsorption capacities were found for well-water from Trenque Lauquen city and tap-water from Buenos Aires city. Both of these samples contained the lowest amount of sulfate and nitrate, explaining the relatively high adsorption capacity. Well-water from Pehuajó city showed a lower q_{eq} than the previously mentioned water samples probably due to a higher sulfate content. Even though the water samples from Tortuguitas city and Chascomús contained lower sulfate contents than Pehuajó city, their nitrate content was five and seven times greater respectively. This could explain the drop in adsorption capacity in those two samples compared with the latter. The lowest q_{eq} were found for the well-water from Chivilcoy city which presented the highest levels of the three anions. The adsorption performance was also analyzed by means of the sorbent dose. For the water samples from Pehuajó the use two and four times the initial sorbent dose showed to increase the total sorption capacity, achieving adsorption levels up to 77% compared with ultrapure water. This suggests that the adsorption percentage of a given natural water sample could be improved by increasing the sorbent dose and therefore overcome the interference of the anions present in some natural waters.

3.8. Sorbent reutilization

In order to assess the feasibility of reutilization of the material, Chi:Ti (5:1) hybrid gels were subjected to a series of adsorption/desorption cycles. As it can be seen in Fig. 6, the initial adsorption capacity is maintained at least up to five cycles, showing not to be significantly different (One-way ANOVA, $p < 0.05$). This was possible due to the chemical stability of the hybrid, which allowed the desorption of the sorbate in alkaline media without affecting the material properties. In alkaline media the TiO_2 surface becomes negatively charged and As(V) anions are displaced by OH^-, clearing the adsorption sites to be equilibrated by water in the equilibration step before the subsequent adsorption cycle.

4. Conclusion

In this work a hybrid hydrogel was obtained by combining chitin with TiO_2 nanoparticles. The resulting material is reinforced with respect to the chitin hydrogel by the nanoparticles which act as fillers. Moreover, the addition of TiO_2 endowed the hybrid with As(V) adsorption capacity. Sorption capacity was found greater at pH below the PZC_{pH} of TiO_2 where the nanoparticles present a surface with positive charge density and the As(V) appears as an anion. In this system, equilibrium was achieved within 4 h following an Elovich model behavior, typical of chemisorption processes. The equilibrium assays showed a consistent behavior of a homogeneous sorbate–sorbent interaction by presenting a better adjustment to the Langmuir model and a value near to 1 for the homogeneity/heterogeneity parameters of the Sips, Toth and Redlich–Peterson models. Typical natural water ions showed to compete with As(V) for the sorption sites, being sulfate the most

Table 3
As(V) adsorption performance of Chi:Ti hybrid in natural water samples.

Sample type	Origin (city)	Initial As(V) (μg/L)	Adsorption (%)	q_{eq} (μg/g)	Cl^- (mg/L)	SO_4^{2-} (mg/L)	NO_3^- (mg/L)
Well	Trenque Lauquen	163 ± 5[a]	49 ± 5	224 ± 8	73.5 ± 0.1	14.1 ± 0.1	6.2 ± 0.1
Tap	Buenos Aires	106 ± 2[a]	34.5 ± 0.9	76 ± 5	21.7 ± 0.7	19 ± 1	–[b]
Well	Pehuajó	103 ± 3[c]	28.8 ± 0.2	46.1 ± 0.5	61.4 ± 0.1	23.5 ± 0.2	8.2 ± 0.1
Well	Tortuguitas	31 ± 1[c]	22.2 ± 0.5	15.4 ± 0.6	44.9 ± 0.6	11.0 ± 0.2	47.7 ± 0.6
Well	Chascomús	115 ± 3[c]	14 ± 5	47 ± 2	19 ± 2	2.03 ± 0.01	71.5 ± 0.1
Well	Chivilcoy	140 ± 5[c]	12.1 ± 0.5	44 ± 2	145 ± 3	76 ± 1	70 ± 5
Well	Pehuajó × 2 S.D.[d]	103 ± 3[c]	40 ± 2	44.4 ± 0.5	61.4 ± 0.1	23.5 ± 0.2	8.2 ± 0.1
Well	Pehuajó × 4 S.D.	103 ± 3[c]	76.7 ± 0.3	52.7 ± 0.2	61.4 ± 0.1	23.5 ± 0.2	8.2 ± 0.1

[a] Spiked.
[b] Not detected.
[c] Natural arsenic.
[d] Sorbent dose.

relevant interference. This interference was also evidenced in As(V) adsorption from natural water samples where the sorption capacity varied depending on the anion composition of the sample. The material also proved that it can be reutilized with the aid of As(V) desorption in alkaline media.

Acknowledgments

M.L.P.R. is grateful for his undergraduate fellowship granted by Universidad de Buenos Aires. J.A.G. is grateful for his doctoral fellowship granted by Universidad de Buenos Aires. M.E.V. is grateful for her doctoral fellowship granted by Consejo Nacional de Investigaciones Científicas y Técnicas. The authors are grateful to the Brazilian Synchrotron Light Laboratory (LNLS) for SAXS facilities. This work was supported with grants from Universidad de Buenos Aires (UBACYT 20020130100780BA) and Consejo Nacional de Investigaciones Científicas y Técnicas (PIP 11220120100657CO). The authors would like to thank I. Pickering for language corrections.

Appendix A. Supplementary data

Supplementary data associated with this article can be found, in the online version, at http://dx.doi.org/10.1016/j.cej.2015.10.035.

References

[1] X. Zhao, L. Lv, B. Pan, W. Zhang, S. Zhang, Q. Zhang, Polymer-supported nanocomposites for environmental application: a review, Environ. Nanotechnol. 170 (2011) 381–394.
[2] I.K. Levy, M. Mizrahi, G. Ruano, G. Zampieri, F.G. Requejo, M.I. Litter, TiO_2-photocatalytic reduction of pentavalent and trivalent arsenic: production of elemental arsenic and arsine, Environ. Sci. Technol. 46 (2012) 2299–2308.
[3] X. Cai, Y. Li, J. Guo, S. Liu, P. Na, Mn(IV) promotion mechanism for the photocatalytic oxidation of arsenite by anatase-TiO_2, Chem. Eng. J. 248 (2014) 9–17.
[4] P.K. Dutta, A.K. Ray, V.K. Sharma, F.J. Millero, Adsorption of arsenate and arsenite on titanium dioxide suspensions, J. Colloid Interface Sci. 278 (2004) 270–275.
[5] L. Yan, Y. Huang, J. Cui, C. Jing, Simultaneous As(III) and Cd removal from copper smelting wastewater using granular TiO_2 columns, Water Res. 68 (2015) 572–579.
[6] X. Guan, J. Du, X. Meng, Y. Sun, B. Sun, Q. Hu, Application of titanium dioxide in arsenic removal from water: a review, J. Hazard. Mater. 215–216 (2012) 1–16.
[7] R. Jayakumar, R. Ramachandran, V.V. Divyarani, K.P. Chennazhi, H. Tamura, S.V. Nair, Fabrication of chitin–chitosan/nano TiO_2-composite scaffolds for tissue engineering applications, Int. J. Biol. Macromol. 48 (2011) 336–344.
[8] Y. Li, J.R. Liu, S.Y. Jia, J.W. Guo, J. Zhuo, P. Na, TiO_2 pillared montmorillonite as a photoactive adsorbent of arsenic under UV irradiation, Chem. Eng. J. 191 (2012) 66–74.
[9] V. Saucedo-Rivalcoba, A.L. Martínez-Hernández, G. Martínez-Barrera, C. Velasco-Santos, J.L. Rivera-Armenta, V.M. Castaño, Removal of hexavalent chromium from water by polyurethane–keratin hybrid membranes, Water Air Soil Pollut. 218 (2011) 557–571.
[10] M. Wysokowski, Ł. Klapiszewski, D. Moszyński, P. Bartczak, T. Szatkowski, I. Majchrzak, et al., Modification of chitin with kraft lignin and development of new biosorbents for removal of cadmium(II) and nickel(II) ions, Mar. Drugs 12 (2014) 2245.
[11] X. Li, H. Zhou, W. Wu, S. Wei, Y. Xu, Y. Kuang, Studies of heavy metal ion adsorption on chitosan/sulfydryl-functionalized graphene oxide composites, J. Colloid Interface Sci. 448 (2015) 389–397.
[12] S. Zhang, F. Xu, Y. Wang, W. Zhang, X. Peng, F. Pepe, Silica modified calcium alginate–xanthan gum hybrid bead composites for the removal and recovery of Pb(II) from aqueous solution, Chem. Eng. J. 234 (2013) 33–42.
[13] H. Tamura, H. Nagahama, S. Tokura, Preparation of chitin hydrogel under mild conditions, Cellulose 13 (2006) 357–364.
[14] X. Hu, Y. Du, Y. Tang, Q. Wang, T. Feng, J. Yang, et al., Solubility and property of chitin in NaOH/urea aqueous solution, Carbohydr. Polym. 70 (2007) 451–458.
[15] R. Muzzarelli, Chitin and its derivatives: new trends of applied research, Carbohydr. Polym. 3 (1983) 53–75.
[16] H. Ehrlich, P. Simon, M. Motylenko, M. Wysokowski, V.V. Bazhenov, R. Galli, et al., Extreme biomimetics: formation of zirconium dioxide nanophase using chitinous scaffolds under hydrothermal conditions, J. Mater. Chem. B 1 (2013) 5092–5099.
[17] M. He, Z. Wang, Y. Cao, Y. Zhao, B. Duan, Y. Chen, et al., Construction of chitin/PVA composite hydrogels with jellyfish gel-like structure and their biocompatibility, Biomacromolecules 15 (2014) 3358–3365.
[18] M. Liu, Y. Zhang, J. Li, C. Zhou, Chitin-natural clay nanotubes hybrid hydrogel, Int. J. Biol. Macromol. 58 (2013) 23–30.
[19] K. Madhumathi, P.T. Sudheesh Kumar, S. Abhilash, V. Sreeja, H. Tamura, K. Manzoor, et al., Development of novel chitin/nanosilver composite scaffolds for wound dressing applications, J. Mater. Sci. Mater. Med. 21 (2010) 807–813.
[20] J.A. Gonzalez, M.F. Mazzobre, M.E. Villanueva, L.E. Diaz, G.J. Copello, Chitin hybrid materials reinforced with graphene oxide nanosheets: chemical and mechanical characterisation, RSC Adv. 4 (2014) 16480–16488.
[21] J.A. González, M.E. Villanueva, L.L. Piehl, G.J. Copello, Development of a chitin/graphene oxide hybrid composite for the removal of pollutant dyes: adsorption and desorption study, Chem. Eng. J. 280 (2015) 41–48.
[22] J.D. Ferry, Viscoelastic Properties of Polymers, third ed., John Wiley & Sons, 1980.
[23] J. Brugnerotto, J. Lizardi, F.M. Goycoolea, W. Argüelles-Monal, J. Desbrières, M. Rinaudo, An infrared investigation in relation with chitin and chitosan characterization, Polymer 42 (2001) 3569–3580.
[24] J. Kohlbrecher, SASfit, Paul Scherrer Institute, Villigen, Switzerland, n.d. <https://kur.web.psi.ch/sans1/SANSSoft/sasfit.html>.
[25] S. Giorgieri, K. Pañak, O. Ruiz, E. Diaz, Monitoreo rápido de aniones y cationes en aguas minerales comerciales mediante el uso de la electroforesis capilar zonal, Quím. Ind. 330 (1997) 42–44.
[26] R Development Core Team, R: A Language and Environment for Statistical Computing, R Foundation for Statistical Computing, Vienna, Austria, 2009. <http://www.R-project.org>.
[27] F.G. Pearson, R.H. Marchessault, C.Y. Liang, Infrared spectra of crystalline polysaccharides. V. Chitin, J. Polym. Sci. 43 (1960) 101–116.
[28] Z. Li, B. Hou, Y. Xu, D. Wu, Y. Sun, W. Hu, et al., Comparative study of sol–gel-hydrothermal and sol–gel synthesis of titania–silica composite nanoparticles, J. Solid State Chem. 178 (2005) 1395–1405.
[29] S. Choudhary, S.R. Bhatia, Rheology and nanostructure of hydrophobically modified alginate (HMA) gels and solutions, Carbohydr. Polym. 87 (2012) 524–530.
[30] G. Beaucage, Small-angle scattering from polymeric mass fractals of arbitrary mass-fractal dimension, J. Appl. Crystallogr. 29 (1996) 134–146.
[31] G. Beaucage, Approximations leading to a unified exponential/power-law approach to small-angle scattering, J. Appl. Crystallogr. 28 (1995) 717–728.
[32] Y.C. Wong, Y.S. Szeto, W.H. Cheung, G. McKay, Sorption kinetics for the removal of dyes from effluents onto chitosan, J. Appl. Polym. Sci. 109 (2008) 2232–2242.
[33] Y.S. Ho, G. McKay, The kinetics of sorption of divalent metal ions onto sphagnum moss peat, Water Res. 34 (2000) 735–742.
[34] S. Kuo, E.G. Lotse, Kinetics of phosphate adsorption and desorption by hematite and gibbsite1, Soil Sci. 116 (1973).
[35] M. Hadi, M.R. Samarghandi, G. McKay, Equilibrium two-parameter isotherms of acid dyes sorption by activated carbons: study of residual errors, Chem. Eng. J. 160 (2010) 408–416.
[36] W.A. Morais, A.L.P. Fernandes, T.N.C. Dantas, M.R. Pereira, J.L.C. Fonseca, Sorption studies of a model anionic dye on crosslinked chitosan, Colloids Surf. Physicochem. Eng. Aspects 310 (2007) 20–31.
[37] S.-Y. Suen, A comparison of isotherm and kinetic models for binary-solute adsorption to affinity membranes, J. Chem. Technol. Biotechnol. 65 (1996) 249–257.
[38] S.S. Barton, Adsorption from dilute, binary, aqueous solutions, J. Colloid Interface Sci. 158 (1993) 64–70.
[39] C.-T. Hsieh, H. Teng, Langmuir and Dubinin–Radushkevich analyses on equilibrium adsorption of activated carbon fabrics in aqueous solutions, J. Chem. Technol. Biotechnol. 75 (2000) 1066–1072.
[40] D. Kumar, L.K. Pandey, J.P. Gaur, Evaluation of various isotherm models, and metal sorption potential of cyanobacterial mats in single and multi-metal systems, Colloids Surf. B 81 (2010) 476–485.
[41] J. Toth, Adsorption: Theory, Modeling and Analysis, Marcel Dekker, New York, 2002.
[42] S. Vasiliu, I. Bunia, S. Racovita, V. Neagu, Adsorption of cefotaxime sodium salt on polymer coated ion exchange resin microparticles: kinetics, equilibrium and thermodynamic studies, Carbohydr. Polym. 85 (2011) 376–387.